

Kinetic Modeling Analysis of Ar Addition to Atmospheric Pressure N₂-H₂ Plasma for Plasma-Assisted Catalytic Synthesis of NH₃

Zihan Lin^a, Shota Abe^{a,b}, Zhe Chen^a, Surabhi Jaiswal^a, and Bruce E. Koel^{a,*}

^aDepartment of Chemical and Biological Engineering, Princeton University, Princeton, NJ 08544, USA

^bPrinceton Plasma Physics Laboratory, 100 Stellarator Road, Princeton, NJ 08540, USA

*Corresponding author: bkoel@princeton.edu

Abstract

Zero-dimensional kinetic modeling of atmospheric pressure Ar-N₂-H₂ nonthermal plasma was carried out to gain mechanistic insights into ammonia formation during plasma-assisted catalysis of ammonia synthesis. The kinetic model was developed for a coaxial dielectric barrier discharge (DBD) quartz wool-packed bed reactor operating at near room temperature using a kHz-frequency plasma source. With 30% Ar mixed in a 1:1 N₂-H₂ plasma at 760 Torr, we find that NH₃ production is dominated by Eley-Rideal (E-R) surface reactions, which heavily involve surface NH_x species derived from N and H radicals in the gas phase, while the influence of excited N₂ molecules is negligible. This is contrary to the commonly proposed mechanism that excited N₂ molecules created by Penning excitation of N₂ by Ar (4s) and Ar(4p) plays a significant role in assisting NH₃ formation. Our model shows that the enhanced NH₃ formation upon Ar dilution is unlikely due to the interactions between Ar and H species, as excited Ar atoms have a weak effect on H radical formation through H₂ dissociation compared to electrons. We find that excited Ar atoms contribute to 28% of the N radical production in the gas phase via N₂ dissociation, while the rest is dominated

by electron-impact dissociation. Furthermore, Ar species play a negligible role in the product NH_3 dissociation. N_2 conversion sensitivity analyses were carried out for electron density (n_e) and reduced electric field (E/N), and contributions from Ar to gas-phase N radical production were quantified. The model can provide guidance on potential reasons for observing enhanced NH_3 formation upon Ar dilution in N_2 - H_2 plasmas beyond changes to the discharge characteristics.

1. Introduction

Ammonia is an essential chemical that is heavily used in industrial and agricultural applications. The world currently produces 130 million tons of NH_3 annually, most of which is used as a precursor for the synthesis of fertilizers.¹ Current industrial processes for synthesizing ammonia are carried out via the traditional Haber-Bosch process, an energy-intensive approach that relies on elevated temperature (400–500 °C) to increase the reaction rate for NH_3 production to a desirable value and high pressure (100–200 bar) to increase the NH_3 equilibrium concentration. Given the extreme conditions, industrial ammonia synthesis accounts for 1-2% of total world energy consumption while emitting 300 million metric tons of CO_2 annually.²

Plasma-assisted catalysis using nonthermal plasma is a promising approach to circumvent the high temperature and pressure required for thermal catalysis through plasma-catalyst synergies. A nonthermal plasma discharge can produce highly reactive species in the gas phase (radicals, ions, free electrons, and excited species) that can undergo reactions at ambient temperature. Most of the energy dissipated to drive a discharge is deposited into free electrons, which generate reactive species through excitation, ionization, and dissociation.³ In recent years, dielectric barrier discharges (DBD) have become ubiquitous in plasma-assisted catalysis studies due to the effective generation of energetic electrons (1-10 eV) and excited species, and

geometric flexibility.⁴ In ammonia synthesis, emphasis has been placed on overcoming the N₂ dissociation barrier, the rate-limiting step in traditional thermal catalysis.⁵ To this end, Mehta et al. proposed that a more energetically efficient pathway is attainable via the adsorption of vibrationally excited N₂ molecules on catalytic sites, thereby lowering the energy barrier for N₂ dissociation.⁶ Alternatively, a less energetically favored approach that has been observed is to produce N radicals by direct N₂ dissociation in the plasma.⁷ Substantial efforts have been devoted to advancing the plasma-assisted catalytic synthesis of ammonia, especially by studying novel catalysts to achieve a higher energy yield.^{2,8-16}

Altering plasma discharge properties via noble gas addition is a well-known concept in surface etching and plasma processing applications.¹⁷⁻¹⁹ Argon plasmas are populated with a high concentration of active species such as metastable Ar, which has a high capability for storing excess energy. Due to their long lifetimes, these metastable states may activate other gaseous species via Penning excitation and ionization processes.²⁰⁻²² Noble gas addition can also stabilize the plasma discharge and offer better control over plasma properties.^{19,23} These concepts have been applied in different types of discharges for plasma-assisted ammonia synthesis. Nakajima and Sekiguchi reported an increased NH₃ formation rate upon argon addition in a microwave discharge.²⁴ Liu et al. found enhanced N₂ conversion by diluting an N₂-H₂ plasma with up to 30% argon in a quartz wool-packed atmospheric pressure DBD reactor.²⁵ In a completely different application, such discoveries have also motivated the investigation of ammonia formation on tungsten and stainless steel surfaces for fusion energy applications.²⁶ Proposed mechanisms for the argon-initiated enhancement of NH₃ formation in the gas phase are the production of active N species via Penning excitation,



and dissociation reactions by excited Ar species,²⁵



An alternative explanation was offered by Nakajima and Sekiguchi, who attributed their observation to charge transfer between Ar^+ and N_2 , which occurs readily due to their similar ionization energies (~ 15.7 eV).^{24,26,27} However, details of the plasma chemistry resulting in ammonia synthesis are not clear in atmospheric pressure Ar- N_2 - H_2 discharges, and experimental results have had limited help from theoretical explanations of modeling studies of Ar- N_2 and Ar- H_2 plasma discharges for different applications.²⁷⁻³⁰ Extensive kinetic modeling for N_2 - H_2 plasma was conducted by Hong et al. to elucidate important mechanisms for plasma-assisted ammonia synthesis.¹ Sode et al. previously modeled low-pressure inductively coupled Ar- N_2 - H_2 plasma with only 1% Ar dilution.³¹ Yet, no atmospheric pressure Ar- N_2 - H_2 plasma modeling of chemical pathways has been investigated to validate proposed mechanisms that facilitate NH_3 formation.

In this article, we report an analysis of the role of argon in the dominant reaction pathway for ammonia synthesis in a DBD flow reactor packed with quartz wool. We adapted the N_2 - H_2 nonthermal plasma model from Hong et al.¹ for understanding ammonia synthesis, consistent with two previous studies from our group on plasma-assisted catalytic synthesis of ammonia in a DBD coaxial flow reactor.^{15,16} Herein, we expanded the N_2 - H_2 nonthermal plasma kinetic model¹ by including Ar plasma chemistry. We compared our calculated N_2 conversions to existing

experimental data to benchmark our results. Detailed pathways for N₂ conversion and Ar contributions to NH₃ production were analyzed for various plasma conditions.

2. Methods

We utilized ZDPlasKin, a 0D kinetics solver, to simulate nonthermal Ar-N₂-H₂ plasma chemistry for NH₃ synthesis that allows for reactions both in the gas phase and on solid surfaces.³²

ZDPlasKin is integrated with a built-in software BOLSIG+, a Boltzmann equation solver that calculates electron properties such as the mean electron temperature and the electron energy distribution function, as well as rate constants of reactions involving electrons.^{33,34} We modified ZDPlasKin to simulate gas flow in a continuously stirred tank reactor (CSTR).¹⁵ Species density evolutions are represented by the CSTR design equation

$$\frac{dn_i}{dt} = \frac{Q}{V}(n_{i,0} - n_i) + \sum_j R_{ij}, \quad (4)$$

where Q is the total input gas flow rate, V is the plasma/reactor volume, $n_{i,0}$ and n_i are the inlet and outlet concentrations of species i expressed in number densities respectively, and R_{ij} is the production rate of species i via reaction j . Based on the existing N₂-H₂ kinetic model^{1,15}, we added Ar species and reactions to our ZDPlasKin CSTR kinetic model, which are listed in Tables 1 and 2, respectively. Ar(meta) and Ar(r) are the 4s excited states. Ar(meta) denotes the 1s³ and 1s⁵ states in Paschen notation. Ar(r) denotes the 1s² and 1s⁴ states. Ar₂^{*} is electronically excited Ar₂. Reactions for N and H species, including interactions between vibrationally and electronically excited species, radicals, ions, and surface species, were adapted from Hong et al.¹ as in our previous reports.^{15,16} In our discussion of excited state chemistry, the electronically

excited N₂ states N₂(C³Π_u), N₂(B³Π_g), and N₂(A³Σ_u⁺) are abbreviated as N₂(C3), N₂(B3) and N₂(A3), respectively.

Table 1. Ar species included in the atmospheric pressure Ar-N₂-H₂ plasma kinetic model in addition to the N and H species given in ref [1].

Neutral atom in ground state	Ions	Excited species
Ar	Ar ⁺ , ArH ⁺ , ArH ₂ ⁺ , ArH ₃ ⁺ , Ar ₂ ⁺ , Ar ₂ H ⁺	Ar(meta), Ar(r), Ar(4p), Ar ₂ [*]

Table 2. Gas-phase reactions utilized in the atmospheric pressure Ar-N₂-H₂ plasma kinetic model in addition to the gas-phase and surface reactions given in ref [1].

No.	Reaction ^a	Rate coefficient (cm ³ s ⁻¹) ^{b,c}	Reference
Electron processes			
R1	$e + \text{Ar} \rightarrow e + e + \text{Ar}^+$	BOLSIG+	33
R2	$e + \text{Ar} \rightarrow e + \text{Ar}(\text{meta})$	$5.0 \times 10^{-9} \times \exp(-12.64/T_e)$	31
R3	$e + \text{Ar} \rightarrow \text{Ar}(\text{r}) + e$	$1.9 \times 10^{-9} \times \exp(-12.6/T_e)$	35
R4	$e + \text{Ar} \rightarrow e + \text{Ar}(4\text{p})$	$2.1 \times 10^{-8} \times \exp(-13.13/T_e)$	35
R5	$e + \text{Ar}^+ \rightarrow \text{Ar}(4\text{p})$	$4 \times 10^{-13} \times T_e^{-0.5}$	36
R6	$e + e + \text{Ar}^+ \rightarrow \text{Ar}(4\text{p}) + e$	$5 \times 10^{-27} \times T_e^{-4.5}$	36
R7	$e + \text{Ar}(\text{meta}) \rightarrow \text{Ar}^+ + e + e$	$1.0 \times 10^{-7} \times \exp(-4.2/T_e)$	35
R8	$e + \text{Ar}(\text{r}) \rightarrow \text{Ar}^+ + e + e$	$1.0 \times 10^{-7} \times \exp(-4.2/T_e)$	35
R9	$e + \text{Ar}(4\text{p}) \rightarrow \text{Ar}^+ + e + e$	$1.8 \times 10^{-7} \times T_e^{0.61} \times \exp(-2.61/T_e)$	35
R10	$e + \text{Ar}(\text{meta}) \rightarrow \text{Ar}(\text{r}) + e$	3.7×10^{-7}	35
R11	$e + \text{Ar}(\text{meta}) \rightarrow \text{Ar}(4\text{p}) + e$	$8.9 \times 10^{-7} \times T_e^{0.51} \times \exp(-1.59/T_e)$	35
R12	$e + \text{Ar}(\text{r}) \rightarrow \text{Ar}(\text{meta}) + e$	9.1×10^{-7}	35
R13	$e + \text{Ar}(\text{r}) \rightarrow \text{Ar}(4\text{p}) + e$	$8.9 \times 10^{-7} \times T_e^{0.51} \times \exp(-1.59/T_e)$	35
R14	$e + \text{Ar}_2^* \rightarrow \text{Ar}_2^+ + e + e$	$9.0 \times 10^{-8} \times T_e^{0.7} \times \exp(-3.66/T_e)$	36
R15	$e + \text{Ar}_2^* \rightarrow \text{Ar} + \text{Ar} + e$	1.0×10^{-7}	36
R16	$e + \text{Ar}_2^+ \rightarrow \text{Ar}(4\text{p}) + \text{Ar}$	$5.4 \times 10^{-8} \times T_e^{-0.66}$	36

R17	$e + \text{ArH}^+ \rightarrow \text{Ar} + \text{H}$	$1.0 \times 10^{-10} \times (-1.5 + 14 \times T_e - 16 \times T_e^2 + 8.4 \times T_e^3 - 1.9 \times T_e^4 + 0.2 \times T_e^5 - 0.0082 \times T_e^6)$	37
Radiative relaxation			
R18	$\text{Ar}(r) \rightarrow \text{Ar}$	1.0×10^5	31
R19	$\text{Ar}(4p) \rightarrow \text{Ar}(r)$	3×10^7	31
R20	$\text{Ar}(4p) \rightarrow \text{Ar}(\text{meta})$	3×10^7	31
Ar ion reactions			
R21	$\text{H}_2^+ + \text{Ar} \rightarrow \text{ArH}^+ + \text{H}$	2.10×10^{-9}	31
R22	$\text{H}_2^+ + \text{Ar} \rightarrow \text{Ar}^+ + \text{H}_2$	2.00×10^{-10}	31
R23	$\text{H}_3^+ + \text{Ar} \rightarrow \text{ArH}^+ + \text{H}_2$	3.70×10^{-10}	31
R24	$\text{Ar}^+ + \text{H}_2 \rightarrow \text{ArH}^+ + \text{H}$	8.7×10^{-10}	31
R25	$\text{Ar}^+ + \text{H}_2 \rightarrow \text{H}_2^+ + \text{Ar}$	1.8×10^{-11}	31
R26	$\text{Ar}^+ + \text{H}_2 \rightarrow \text{Ar} + \text{H}^+ + \text{H}$	1.0×10^{-9}	36
R27	$\text{Ar}^+ + \text{H} \rightarrow \text{H}^+ + \text{Ar}$	1.0×10^{-10}	36
R28	$\text{Ar}^+ + \text{N}_2 \rightarrow \text{N}_2^+ + \text{Ar}$	4.45×10^{-10}	35
R29	$\text{Ar}^+ + \text{N}_2 \rightarrow \text{Ar} + \text{N}^+ + \text{N}$	5.0×10^{-12}	36
R30	$\text{Ar}^+ + \text{N} \rightarrow \text{Ar} + \text{N}^+$	4.45×10^{-10}	27
R31	$\text{Ar}^+ + \text{NH}_2 \rightarrow \text{NH}^+ + \text{H} + \text{Ar}$	5.5×10^{-11}	36
R32	$\text{Ar}^+ + \text{NH}_3 \rightarrow \text{NH}_3^+ + \text{Ar}$	$1.84 \times 10^{-9} \times 0.92$	38
R33	$\text{Ar}^+ + \text{NH}_3 \rightarrow \text{NH}_2^+ + \text{H} + \text{Ar}$	$1.84 \times 10^{-9} \times 0.03$	38
R34	$\text{Ar}^+ + \text{NH}_3 \rightarrow \text{ArH}^+ + \text{NH}_2$	$1.84 \times 10^{-9} \times 0.05$	38
R35	$\text{Ar}^+ + \text{Ar} \rightarrow \text{Ar} + \text{Ar}^+$	4.6×10^{-10}	36
R36	$\text{N}^+ + \text{Ar} \rightarrow \text{N} + \text{Ar}^+$	6.0×10^{-14}	27
R37	$\text{N}_2^+ + \text{Ar} \rightarrow \text{Ar}^+ + \text{N}_2$	2.81×10^{-10}	27
R38	$\text{N}_3^+ + \text{Ar} \rightarrow \text{N}_2 + \text{N} + \text{Ar}^+$	6.6×10^{-11}	27
R39	$\text{N}_4^+ + \text{Ar} \rightarrow \text{Ar}^+ + \text{N}_2 + \text{N}_2$	1.0×10^{-11}	27
R40	$\text{Ar}_2^+ + \text{N}_2 \rightarrow \text{Ar}^+ + \text{Ar} + \text{N}_2$	2.50×10^{-10}	38
R41	$\text{Ar}_2^+ + \text{H}_2 \rightarrow \text{ArH}^+ + \text{Ar} + \text{H}$	4.7×10^{-10}	38
R42	$\text{Ar}_2^+ + \text{H} \rightarrow \text{H}^+ + \text{Ar} + \text{Ar}$	5.0×10^{-11}	36
R43	$\text{ArH}^+ + \text{H}_2 \rightarrow \text{H}_3^+ + \text{Ar}$	6.3×10^{-10}	31
R44	$\text{ArH}_2^+ + \text{H}_2 \rightarrow \text{ArH}_3^+ + \text{H}$	1.19×10^{-9}	38
R45	$\text{Ar}_2\text{H}^+ + \text{H}_2 \rightarrow \text{ArH}_3^+ + \text{Ar}$	1.20×10^{-10}	38
R46	$\text{ArH}^+ + \text{NH}_3 \rightarrow \text{NH}_3^+ + \text{H} + \text{Ar}$	5.3×10^{-10}	31
R47	$\text{ArH}^+ + \text{NH}_3 \rightarrow \text{NH}_4^+ + \text{Ar}$	1.6×10^{-9}	31

R48	$\text{ArH}^+ + \text{N}_2 \rightarrow \text{N}_2\text{H}^+ + \text{Ar}$	8.0×10^{-10}	31
R49	$\text{ArH}_3^+ + \text{N}_2 \rightarrow \text{N}_2\text{H}^+ + \text{Ar} + \text{H}_2$	9.0×10^{-10}	38
R50	$\text{ArH}_3^+ + \text{NH}_3 \rightarrow \text{NH}_4^+ + \text{Ar} + \text{H}_2$	2.56×10^{-9}	38
R51	$\text{H}^- + \text{Ar}_2^+ \rightarrow \text{H} + \text{Ar} + \text{Ar}$	2.0×10^{-7}	36
R52	$\text{H}^- + \text{ArH}^+ \rightarrow \text{H} + \text{H} + \text{Ar}$	2.0×10^{-7}	36
Excited Ar and neutral reactions			
R53	$\text{Ar}(\text{meta}) + \text{Ar}(\text{meta}) \rightarrow \text{Ar}^+ + \text{Ar} + e$	6.4×10^{-10}	35
R54	$\text{Ar}(\text{meta}) + \text{Ar}(4\text{p}) \rightarrow \text{Ar}^+ + \text{Ar} + e$	1.0×10^{-9}	36
R55	$\text{Ar}(\text{meta}) + \text{Ar}(\text{r}) \rightarrow \text{Ar}^+ + \text{Ar} + e$	2.1×10^{-9}	35
R56	$\text{Ar}(\text{meta}) + \text{N}_2 \rightarrow \text{N} + \text{N} + \text{Ar}$	1.6×10^{-11}	35
R57	$\text{Ar}(\text{meta}) + \text{H}_2 \rightarrow \text{H} + \text{H} + \text{Ar}$	1.1×10^{-10}	31
R58	$\text{Ar}(\text{r}) + \text{N}_2 \rightarrow \text{Ar} + \text{N} + \text{N}$	1.6×10^{-11}	35
R59	$\text{Ar}(\text{r}) + \text{H}_2 \rightarrow \text{Ar} + \text{H} + \text{H}$	1.1×10^{-10}	31
R60	$\text{Ar}(\text{r}) + \text{Ar}(4\text{p}) \rightarrow \text{Ar}^+ + \text{Ar} + e$	1.0×10^{-9}	36
R61	$\text{Ar}(4\text{p}) + \text{Ar}(4\text{p}) \rightarrow \text{Ar}^+ + \text{Ar} + e$	1.0×10^{-9}	36
R62	$\text{Ar}_2^* + \text{H}_2 \rightarrow \text{H} + \text{H} + \text{Ar} + \text{Ar}$	7.6×10^{-11}	39
R63	$\text{Ar}_2^* + \text{Ar}_2^* \rightarrow \text{Ar}_2^+ + \text{Ar} + \text{Ar} + e$	5.0×10^{-10}	36
R64	$\text{Ar}_2^* \rightarrow \text{Ar} + \text{Ar}$	6.0×10^7	36
R65	$\text{Ar} + \text{N}_2 \rightarrow \text{N} + \text{N} + \text{Ar}$	$4.3 \times 10^{-10} \times \exp(-86460/T_g)$	36
R66	$\text{N}_2(\text{B3}) + \text{Ar} \rightarrow \text{N}_2(\text{A3}) + \text{Ar}$	3.0×10^{-13}	35
R67	$\text{N}_2(\text{a'1}) + \text{Ar} \rightarrow \text{N}_2(\text{B3}) + \text{Ar}$	1.0×10^{-14}	35
Penning excitation			
R68	$\text{Ar}(\text{meta}) + \text{N}_2 \rightarrow \text{N}_2(\text{C3}) + \text{Ar}$	3.0×10^{-11}	30
R69	$\text{Ar}(\text{meta}) + \text{N}_2 \rightarrow \text{N}_2(\text{B3}) + \text{Ar}$	9.8×10^{-12}	30
R70	$\text{Ar}(\text{r}) + \text{N}_2 \rightarrow \text{N}_2(\text{C3}) + \text{Ar}$	3.0×10^{-11}	30
R71	$\text{Ar}(\text{r}) + \text{N}_2 \rightarrow \text{N}_2(\text{B3}) + \text{Ar}$	9.8×10^{-12}	30
Recombination			
R72	$\text{N} + \text{N} + \text{Ar} \rightarrow \text{N}_2 + \text{Ar}$	2.3×10^{-32}	36
R73	$\text{H} + \text{H} + \text{Ar} \rightarrow \text{H}_2 + \text{Ar}$	$6.4 \times 10^{-33} \times (300/T_g)$	36
R74	$\text{N}^+ + \text{N} + \text{Ar} \rightarrow \text{N}_2^+ + \text{Ar}$	1.0×10^{-29}	35
R75-77	$\text{Ar} + \text{Ar} + \text{M} \rightarrow \text{Ar}_2^* + \text{Ar}$	1.1×10^{-32}	36
R78	$\text{N} + \text{N} + \text{Ar} \rightarrow \text{N}_2(\text{B3}) + \text{Ar}$	$(2.0/6.5) \times 8.27 \times 10^{-34} \times \exp(500/T_g)$	35
R79	$\text{H} + \text{H} + \text{NH}_3 \rightarrow \text{H}_2 + \text{NH}_3$	1.4×10^{-31}	36

Reactions with NH species			
R80-82	$\text{NH}_3 + \text{M} \rightarrow \text{Ar} + \text{NH}_3^+ + e$	4.2×10^{-11}	36
R83-85	$\text{NH}_3 + \text{M} \rightarrow \text{Ar} + \text{NH}_2 + \text{H}$	5.8×10^{-11}	36
R86-88	$\text{NH}_3 + \text{M} \rightarrow \text{Ar} + \text{NH} + \text{H} + \text{H}$	5.2×10^{-11}	36
R89-91	$\text{NH}_3 + \text{M} \rightarrow \text{Ar} + \text{NH} + \text{H}_2$	5.8×10^{-12}	36
R92	$\text{Ar} + \text{NH}_3 \rightarrow \text{H}_2 + \text{NH} + \text{Ar}$	$1.1 \times 10^{-9} \times \exp(-47032/T_g)$	36
R93	$\text{Ar} + \text{NH}_2 \rightarrow \text{H} + \text{NH} + \text{Ar}$	$2.2 \times 10^{-9} \times \exp(-38224/T_g)$	36
R94	$\text{Ar} + \text{NH} \rightarrow \text{H} + \text{N} + \text{Ar}$	$3.0 \times 10^{-10} \times \exp(-37615/T_g)$	36

^aRate coefficients for three body reactions have units of $\text{cm}^6 \text{s}^{-1}$. For radiation reactions, the units are s^{-1} .

^bM represents Ar(meta), Ar(r), and Ar(4p).

^c T_e is in eV and T_g is in K unless otherwise specified.

Another addition to our previous CSTR ZDPlasKin model¹⁵ is the ambipolar diffusion process to account for the loss of positive ions to the wall, which is described in general as



in ZDPlasKin. The rate coefficients were calculated by³⁰

$$r = \frac{A}{V} \sqrt{\frac{kT_e}{m_i}} \quad (6)$$

where m_i is the species mass, T_e is the electron temperature, k is the Boltzmann constant, V is the volume, and A is the effective surface area. Eley-Rideal (E-R) surface reactions and radical adsorption at surfaces have rate coefficients calculated by

$$k = \left[\frac{\Lambda^2}{D} + \frac{V}{A} \frac{2(2 - \gamma)}{\bar{v}\gamma} \right]^{-1} S_T^{-1}, \quad (7)$$

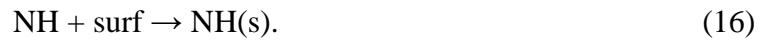
where for the gas phase species, Λ is the diffusion length, D is the diffusion coefficient, γ is the sticking coefficient, and \bar{v} is the thermal velocity; reactor dimensions are defined by V the

discharge volume, A the surface area that the gas species interact with, and S_T the total surface sites in number density. A more detailed discussion of these terms can be found in Chen et al.¹⁵ Combining the discharge volume and effective surface area gives a characteristic length, or the volume-to-surface area ratio (V/A). We excluded Langmuir-Hinshelwood (L-H) reactions since the dissociative adsorption of vibrationally excited N_2 on quartz is unlikely.¹⁶ Moreover, we previously found that E-R reactions occur faster than L-H reactions under typical DBD plasma conditions and that the conditions (low reduced electric field) under which L-H reactions occur faster than E-R reactions and radical adsorption are challenging for plasma generation.^{15,16}

E-R reactions (“surf” denotes a surface site) in our model include



We also included the radical adsorption reactions



N_2 conversion was calculated as

$$\text{N}_2 \text{ conversion} = \frac{n_{\text{NH}_3}}{2n_{\text{N}_2,0}}, \quad (17)$$

where n_{NH_3} is the NH_3 number density in the effluent and $n_{\text{N}_2,0}$ is the N_2 number density in the input for the reactor.

3. Results

3.1. Benchmarking model results and sensitivity analysis

We calculated N_2 conversions for typical input parameters that are reported and characteristic of DBD plasmas used for plasma-assisted catalytic ammonia synthesis. We configured the simulation setup to replicate the coaxial DBD reactor conditions of Liu et al.²⁵ Unless otherwise specified, the reactor conditions are given by the reduced electric field (E/N) = 71 Td, Ar % = 30%, Q = 100 ml/min, V = 1.508 ml, and gas pressure ratio $\text{N}_2:\text{H}_2$ = 1:1. The total gas pressure (P) and gas temperature (T_g) are 760 Torr and 300 K, respectively. The specific input energy, 15 kJ L^{-1} , is defined as the ratio of energy dissipated per minute and gas flow rate. The electron density (n_e) was not reported in Liu et al.²⁵ We examined the range of n_e from 10^6 - 10^9 cm^{-3} that is typically found in packed-bed reactors^{1,15,16} measured by voltage-charge Lissajous plots. Our group also observed n_e values typically on the order of 10^6 - 10^8 cm^{-3} in near-atmospheric pressure Ar- N_2 - H_2 plasmas in an empty tube flow reactor using the Lissajous method. The reactor-dependent parameters of surface-to-area ratio (V/A) and diffusion length (Λ) are important to surface reactions. We used the volume-to-surface area ratio, $V/A = 1 \times 10^{-6} \text{ m}$, estimated from the geometric area, $0.20 \text{ m}^2/\text{g}$, and the density of quartz wool, 2.2 - 2.6 g/cm^3 ,^{40,41} for the reactor used in Liu et al.²⁵ Although the value of V/A from this estimation can be obscured depending on the effective surface area that the plasma species interact with, our previous modeling work found

that N_2 conversion is not sensitive to V/A values once they reach the order of magnitude used for this simulation.¹⁵ The diffusion length (Λ) is challenging to capture because it is also affected by the macroscopic geometrical configuration of the wool fibers. In practice, the space gaps between fibers of quartz wool typically range from 1 to 100 μm .^{42,43}

Fig. 1 shows the calculated N_2 conversions for different electron densities and diffusion lengths. As the electron density increases, we observe increasing N_2 conversion. Liu et al. measured N_2 conversion of 0.18% for an input energy of 15 kJ L^{-1} .²⁵ At $n_e = 1.8 \times 10^8 \text{ cm}^{-3}$, the calculated N_2 conversion matched well their experimental result. The calculated results using three diffusion lengths vary by less than 0.05%. A more detailed sensitivity analysis for the effect of diffusion length on N_2 conversion is illustrated in Fig. 2. The choice of diffusion length does not significantly affect the calculated N_2 conversion over this range and the calculated N_2 conversions vary less than 0.05%.

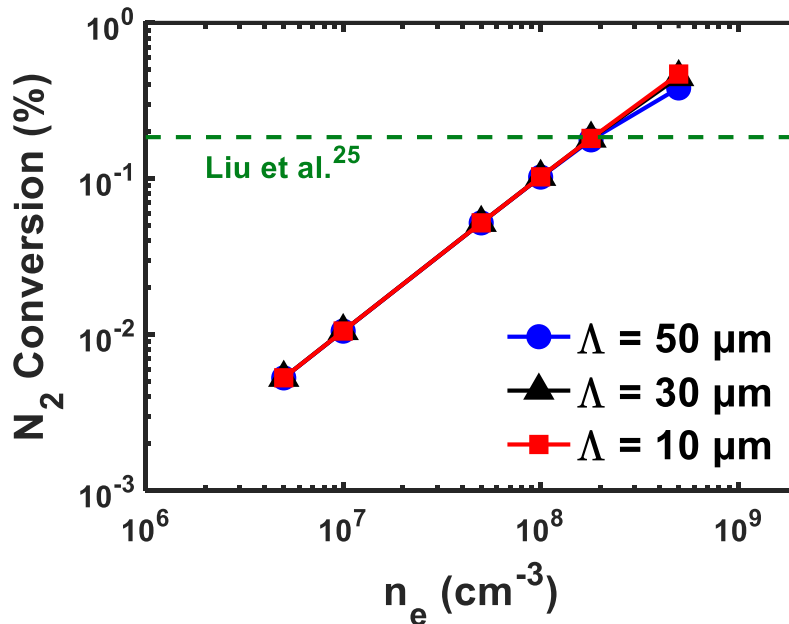


Figure 1. Calculated N_2 conversion as a function of electron density for different diffusion lengths. The dashed line denotes an experimental value from Liu et al.²⁵

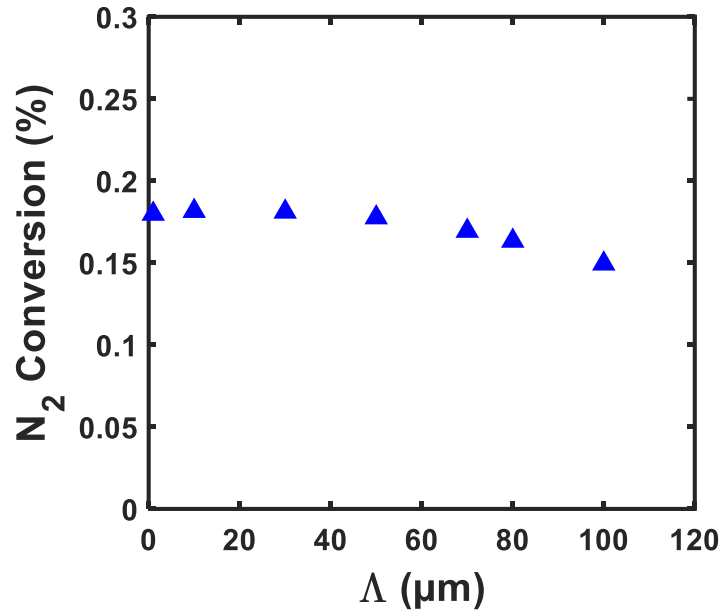


Figure 2. Effect of diffusion length on calculated N_2 conversion. Plasma conditions: $E/N = 71$ Td, $n_e = 1.8 \times 10^8 \text{ cm}^{-3}$.

3.2. Reaction pathways of NH_3 synthesis for an atmospheric pressure Ar- N_2 - H_2 plasma in a quartz wool-packed DBD reactor

The ZDPlasKin CSTR kinetic model constructed as described above was used to identify the major pathways for NH_3 production in an Ar- N_2 - H_2 plasma in a quartz wool-packed DBD reactor under a specific condition of interest. Fig. 3 shows the production rates of major species and reaction pathways for NH_3 production assuming $n_e = 1.8 \times 10^8 \text{ cm}^{-3}$ and $\Lambda = 10 \mu\text{m}$ (Sec. 3.1.). Reactions that were originally included in the ZDPlasKin model in refs. [1] and [15] and are important for NH_3 formation are listed in Table 3. The rates were normalized by the total formation rate of NH_3 via surface pathways, i.e., the sum of rates for R95-97, which are the final steps of producing NH_3 . For the dissociation of N_2 and H_2 , the relative production rate shown in Fig. 3 is double the relative steady-state reaction rate since two N and two H radicals are produced per dissociation reaction of N_2 and H_2 , respectively. E-R reactions account for nearly all of the NH_3 production, where the most dominant is $\text{H}_2 + \text{NH}(\text{s}) \rightarrow \text{NH}_3 + \text{surf}$ (R97, 41% of

NH₃ formation), followed by H + NH₂(s) → NH₃ + surf (R95, 32%) and NH₂ + H(s) → NH₃ + surf (R96, 27%). NH₃ produced from gas-phase radical reactions, i.e., not involving a surface, account for less than 0.4% of the total NH₃ formation.

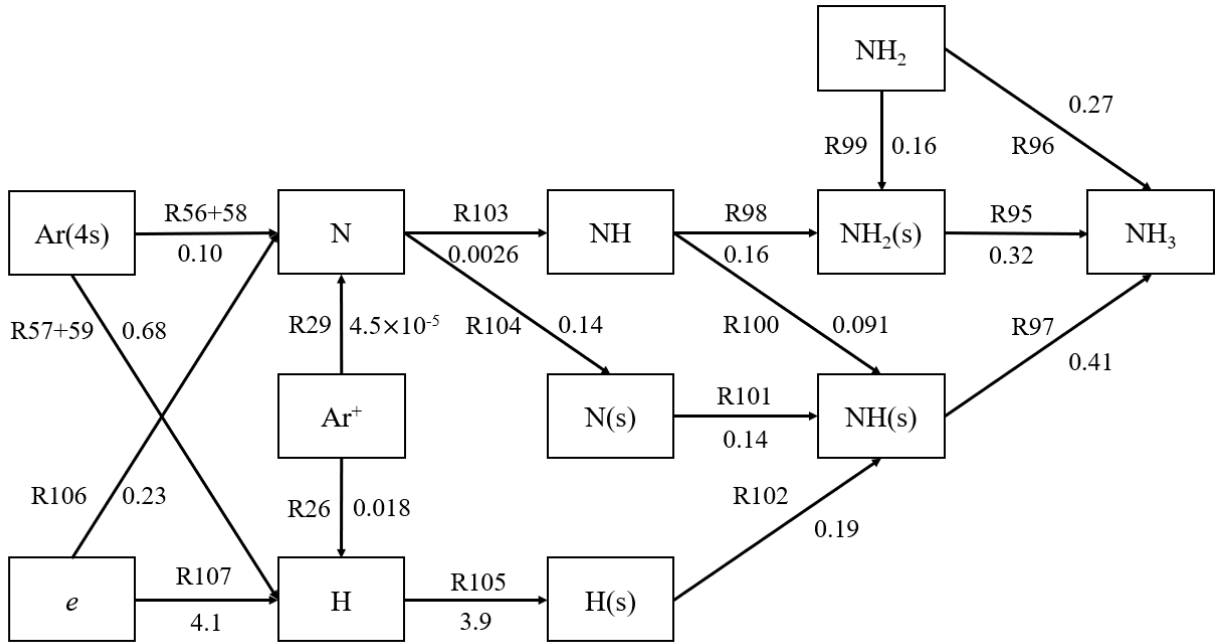
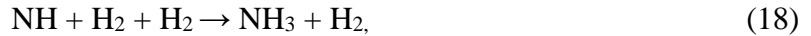


Figure 3. Reaction network for plasma-assisted catalytic NH₃ synthesis in a quartz wool-packed DBD reactor. Simulation conditions: $n_e = 1.8 \times 10^8 \text{ cm}^{-3}$, $E/N = 71 \text{ Td}$, $\Lambda = 10 \text{ }\mu\text{m}$. Production rates were normalized by the total formation rate of NH₃ via the E-R surface reaction pathways (R95-97) in Table 3.

Table 3. Major reactions for NH₃ formation involving N and H species identified for an atmospheric pressure Ar-N₂-H₂ DBD plasma at the conditions of E/N = 71 Td and n_e = 1.8×10⁸ cm⁻³.

No.	Reaction
R95	H + NH ₂ (s) → NH ₃ + surf
R96	NH ₂ + H(s) → NH ₃ + surf
R97	H ₂ + NH(s) → NH ₃ + surf
R98	NH + H(s) → NH ₂ (s)
R99	NH ₂ + surf → NH ₂ (s)
R100	NH + surf → NH(s)
R101	H + N(s) → NH(s)
R102	N + H(s) → NH(s)
R103	N + H ₂ * → NH + H
R104	N + surf → N(s)
R105	H + surf → H(s)
R106	e + N ₂ → e + 2N
R107	e + H ₂ → e + 2H

In the steady state, the production processes of NH(s) rely mainly on gas-phase N and H radicals and adsorbed N and H adatoms (surface-bound atoms). The direct adsorption of gas-phase NH radicals (R100) contributes 22% compared to 33% via the E-R reaction of H + N(s) → NH(s) (R101) and 45% via the E-R reaction of N + H(s) → NH(s) (R102). In the steady state, the dominant route of gas-phase NH radical production is the electron-impact dissociation of NH₃. We note that the reaction between gas-phase N radicals and electronically excited H₂ molecules in the gas phase (R103) only has a relative NH production rate of 0.0026 at steady state. Hong et al. found that gas-phase NH radicals were important in the early phase of NH₃ formation through the three-body gas-phase reactions



which are more prominent at atmospheric pressure than in low-pressure regimes.¹ Gas-phase NH radicals were mainly produced by the electron-impact dissociation of NH₃ after the build-up of

NH₃ in the gas phase, which allows electron-impact dissociation of NH₃ into gas-phase NH_x radicals.

The formation of adsorbed NH(s) via R100-102 and NH radicals in the gas phase via R103 highlights the importance of both gas-phase N radicals and adsorbed N adatoms. We found that gas-phase N radical adsorption and the formation of adsorbed NH(s) by $H + N(s) \rightarrow NH(s)$ have the same relative production rates. This means that adsorbed N adatoms are not depleted by faster side reactions that do not lead to NH₃ formation and promptly contribute via R97 to the NH₃ formation reaction network. We found that excited argon species via R56+58 contribute to 28% of the total gas-phase N radical production, but direct dissociation of gas-phase N₂ molecules by collisions with electrons is the major source of N radicals in the gas phase comprising 65%. Furthermore, the contribution of excited argon species to gas-phase N radical production derives almost completely from Ar(meta) and Ar(r) (the 4s excited states). The relative production rate of gas-phase N radicals via R29 indicates that Ar⁺ has a negligible contribution to the direct dissociation of N₂ in the gas phase. At a low degree of ionization, we expect radicals to play a more significant role than ions. For H radical production, H₂ dissociation by Ar species is only 17% of that caused by electron-impact dissociation. Thus, one potential cause of the slight enhancement of N₂ conversion observed in the experiments of Liu et al.²⁵ is the role of metastable Ar species in dissociating N₂ molecules.

4. Discussion

The zero-dimensional kinetic modeling of atmospheric pressure Ar-N₂-H₂ nonthermal plasma we carried out enables a detailed reaction analysis regarding the effects of Ar addition on ammonia formation in a DBD plasma. Unless otherwise specified, the input plasma parameters for the

discussion below are the same as given herein in Sec. 3.2, i.e., $E/N = 71$ Td, $n_e = 1.8 \times 10^8 \text{ cm}^{-3}$, Ar % = 30%, $Q = 100$ ml/min, $V = 1.508$ ml, $N_2:H_2 = 1:1$, $P = 760$ Torr, and $T_g = 300$ K.

4.1. NH₃ decomposition by argon species

Energy transfer between excited Ar species and NH₃ in the gas phase may result in NH₃ decomposition. The 4s and 4p metastable Ar states have excitation energies of 11.6 and 13.1 eV, respectively, which are sufficient to cause NH₃ dissociation.³⁶ At steady state, NH₃ is predominantly decomposed in the plasma by electron impact with a rate of $7.1 \times 10^{16} \text{ cm}^{-3} \text{ s}^{-1}$, corresponding to 65% of the total NH₃ formation rate via E-R surface reactions. Argon species play a weaker role in NH₃ dissociation. Major argon species that participate in NH₃ decomposition reactions include Ar(meta), Ar(r), Ar(4p), Ar⁺, and ArH⁺. These reactions are described by R80-91 for Ar(meta), Ar(r), and Ar(4p), R32-34 for Ar⁺, and R46-47 for ArH⁺. The contribution from Ar(4p) is the most significant, with a total rate for NH₃ decomposition of $3.2 \times 10^{15} \text{ cm}^{-3} \text{ s}^{-1}$. However, this rate is still 95% slower than electron-impact dissociation of NH₃. Dissociation rates of NH₃ are one order of magnitude lower by Ar(meta) and Ar(r), and three orders of magnitude lower by Ar⁺ and ArH⁺, compared to that by Ar(4p). It is worth noting that dissociation by Ar(meta), Ar(r), Ar(4p), and Ar⁺ can also directly lead to the production of the gas-phase radicals NH and NH₂, which can be utilized to produce NH₂(s) by radical adsorption. We thus conclude that argon does not have a profound effect on the destruction of NH₃ in the plasma.

4.2. The role of Ar⁺ ions and dissociative recombination of N₂⁺ ions

Gas-phase Ar and N₂ have similar first ionization energies (15.76 eV and 15.58 eV).²⁶ Thus, charge transfer between gas-phase Ar and N₂ happens readily in the plasma.²⁸ In steady state, we

found that charge transfer from gas-phase Ar^+ to N_2 (eq. 20) happens four times as fast as the reverse process (eq. 21).



Nakajima et al. proposed that charge transfer reactions enhance gas-phase N radical density in the plasma by the subsequent dissociative recombination of N_2^+ .²⁴ Kang et al. found that the dissociative recombination

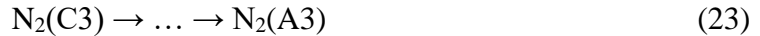


dominates N radical production pathways when Ar is the main discharge gas component in a 200-mTorr Ar- N_2 plasma.²⁸

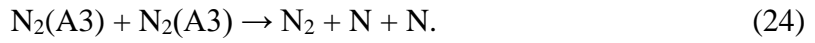
Under the conditions of the calculations herein, the dissociative recombination reactions of N_2^+ are ten orders of magnitude slower than that of electron-impact dissociation of N_2 . We first attributed the observation to our low degree of ionization and an abundance of side reactions enabled by the highly collisional environment at atmospheric pressure. But Liang et al.³⁵ and Bogaerts²⁷ also found the production of gas-phase N radical by the dissociative recombination reactions of N_2^+ is insignificant at low pressure and higher electron density in Ar- N_2 plasma. In our model of an atmospheric pressure Ar- N_2 - H_2 plasma, we found N_2^+ is mostly depleted by collision with H_2 molecules to produce gas-phase N_2H^+ rather than with neutralization by electrons or charge transfer with Ar, and the gas-phase N_2H^+ can subsequently play a minor role in consuming NH_3 via the gas-phase reaction $\text{N}_2\text{H}^+ + \text{NH}_3 \rightarrow \text{NH}_4^+ + \text{N}_2$.

4.3. Penning excitation by argon species

Penning excitation of N₂ in the gas phase by excited Ar species (R68-71) was investigated. The energy transferred from excited Ar species in turn dissipates via reactions and decay processes of electronically excited N₂ species. One such process is the radiative decay from the higher energy state N₂(C3) to the lower energy state N₂(A3) (eq. 23).

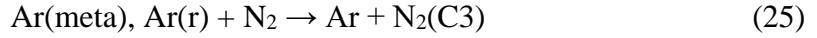


More details regarding the interactions between electronically excited N₂ species can be found in Hong et al.¹ It has also been suggested that metastable-metastable pooling dissociation between two N₂(A3) molecules can effectively generate N radicals in the gas phase via²⁸



However, we found that the rate of N radical production from N₂(A3) dissociation is several orders of magnitude lower than N₂ dissociation by Ar(meta) and Ar(r) under the plasma conditions for ammonia synthesis in Fig. 3. We note that gas-phase Ar(meta) is mostly depleted by collisions with H₂ leading to dissociation (R57), with slower Ar(meta) depletion caused by Penning excitation of N₂ (R68+69) and collisions with N₂ leading to dissociation (R56). Among interactions between Ar(meta) and N₂, the steady state reaction rates for R56, R68, and R69 are $3.1 \times 10^{15} \text{ cm}^{-3} \text{ s}^{-1}$, $5.8 \times 10^{15} \text{ cm}^{-3} \text{ s}^{-1}$, and $1.9 \times 10^{15} \text{ cm}^{-3} \text{ s}^{-1}$, respectively. The utility of Ar(meta) for the Penning excitation of N₂ to produce N₂(B3) and N₂(C3) causes a 2.5 times higher rate of Ar(meta) depletion than collisions with N₂ leading to dissociation of N₂. Yet, the contribution to N₂(C3) production by both Ar(meta) and Ar(r) (eq. 25) is only 8.0% of that caused by electron-

impact excitation (eq. 26). For N₂(B3) formation, the contribution by both Ar(meta) and Ar(r) declines to 1.2% of that caused by electron-impact excitation. The high Penning excitation reaction rates suggest that Penning excitation is a pronounced mechanism for quenching Ar(meta) by N₂, but a minor source of electronically excited N₂ under these conditions.



4.4. N₂ conversion and Ar contribution as affected by electron density and reduced electric field

Fig. 4 shows N₂ conversion as a function of the reduced electric field (E/N) and electron density (n_e). These calculated N₂ conversions are intended to provide guidance for the different plasma conditions needed to determine the optimal operating conditions. N₂ conversion increases with both E/N and n_e, which is expected given the higher input power. Within this range of E/N and n_e values, E-R surface reactions dominate NH₃ formation. The sources of N radicals in the gas phase are dominated by N₂ dissociation by electron impact and collisions with Ar(meta) and Ar(r). We define the Ar contributing factor as the ratio of the rate of N₂ dissociation by both Ar(meta) and Ar(r) to that by electron-impact dissociation (eq. 27).

$$f_{\text{Ar} \rightarrow \text{N}} = \frac{\Gamma_{\text{R56}} + \Gamma_{\text{R58}}}{\Gamma_{\text{R106}}} \quad (27)$$

Fig. 5 gives the Ar contributing factor in atmospheric pressure Ar-N₂-H₂ plasma for the various conditions we simulated. The Ar contributing factor never exceeds 1, indicating that

electron-impact dissociation of N_2 always dominates. In cases when Ar is the dominant gas component in the plasma, N_2 dissociation by excited Ar has been found to surpass electron impact dissociation.^{27,35} Our model predicts that the Ar contributing factor is maximized at $E/N = 80$ Td, when the mean electron temperature is 2.7 eV, and decreases with high n_e .

It is commonly assumed in the literature that the plasma is a source of vibrationally excited N_2 molecules, which can dissociatively adsorb at the catalytic surface via a lower energy barrier, and this enhances the rate of N_2 dissociation, which is the rate-determining step.^{5,6,44} However, due to the reactivity of N radicals, they can outcompete excited N_2 molecules as a source of N(s) on a catalyst.⁷ Engelmann et al. showed that reactions of plasma-generated radicals have more impact on NH_3 formation than catalytic dissociation of excited N_2 molecules in an atmospheric pressure N_2 - H_2 DBD discharge at 400 K and $E/N = 20$ -100 Td.⁴⁵ Although our model shows that Ar(meta) and Ar(r) in the plasma can potentially help promote the generation of gas-phase N radicals and enhance the subsequent E-R reactions to form NH_3 , dissociation of N_2 molecules in the plasma is not catalyzed and inherently more energetically expensive than excitation. Given that electron-impact dissociation of gas-phase N_2 always dominates the production of gas-phase N radicals, the opportunity for diluting N_2 - H_2 plasma with Ar may instead be found in plasma generation and production of excited gas-phase N_2 molecules rather than N_2 dissociation in the plasma. Our model suggests that N_2 molecules can effectively quench Ar(4s) via Penning excitation reactions and produce electronically excited gas-phase N_2 at atmospheric pressure and near room temperature. Akin to vibrationally excited N_2 , dissociative adsorption of electronically excited N_2 may also occur on catalytic sites via a lower energy barrier.¹ Moreover, Ar dilution is known for enhancing the electron density in the plasma and sustaining the host plasma at lower reduced electric fields.^{17,21,25,28} Lower values of E/N (1-30

Td) are also more favorable for the generation of vibrationally excited species compared to that in high E/N regimes.⁴⁶ Therefore, the utilization of Ar to tailor discharge characteristics and produce electronically excited gas-phase N₂ molecules under other plasma conditions are directions that should be investigated. Future studies may also examine conditions in which L-H reactions can compete with E-R reactions over a metal catalyst when Ar is added to N₂-H₂ plasmas.

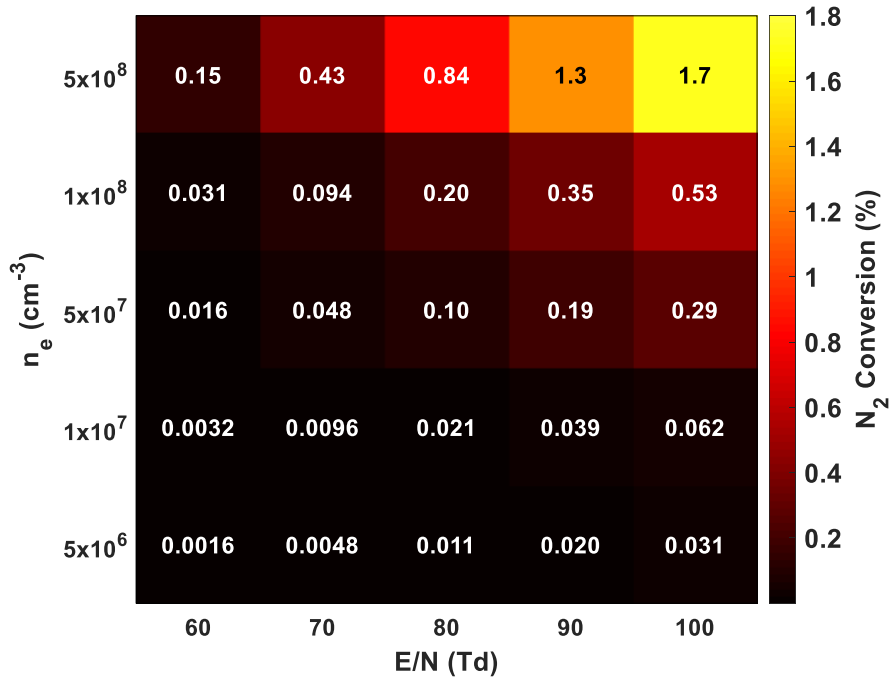


Figure 4. Dependence of N₂ conversion on the reduced electric field and electron density in a 1:1 N₂-H₂ plasma with 30% Ar in a quartz wool-packed DBD reactor at atmospheric pressure and near room temperature.

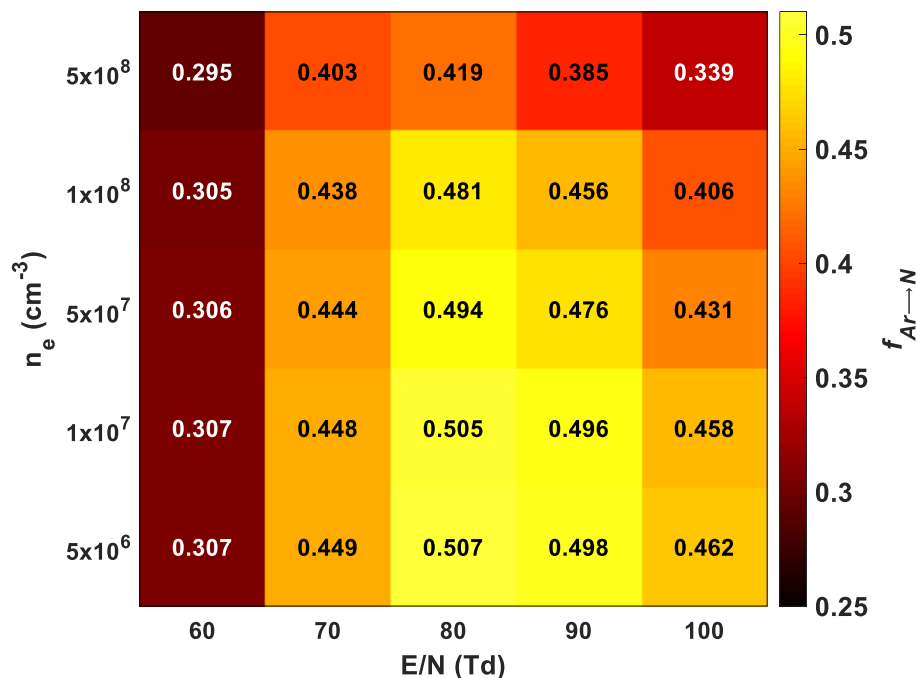


Figure 5. Dependence of the Ar contributing factor on the reduced electric field and electron density in a 1:1 $\text{N}_2\text{-H}_2$ plasma with 30% Ar in a quartz wool-packed DBD reactor at atmospheric pressure and near room temperature. The Ar contributing factor is defined as the ratio of the rate of N_2 dissociation by Ar(meta) and Ar(r) to that by electron-impact dissociation.

5. Conclusion

We have investigated the chemical pathways in atmospheric pressure Ar- $\text{N}_2\text{-H}_2$ nonthermal plasmas for ammonia synthesis by using a 0D nonthermal plasma kinetic model adapted to a coaxial DBD flow reactor packed with quartz wool. By comparing the modeling results with existing experimental results, we identified the target conditions for the analysis of the NH_3 synthesis pathway. It was observed that the model is not sensitive to the choice of diffusion length in the regime that we investigated, which is an important parameter for calculating reaction rates for processes involving the surfaces in the reactor. Upon diluting a 1:1 $\text{N}_2\text{-H}_2$ plasma with 30% Ar, the kinetics of formation of gas-phase N and H radicals and surface-bound N and H adatoms are supplemented by reactions of gas-phase N_2 and H_2 with excited Ar species. Under the conditions that we identified, we found that Ar can contribute to 28% of N radical

production in the gas phase, which subsequently produces gas-phase NH radicals and adsorbed $\text{NH}_x(\text{s})$ species in the early steps of NH_3 synthesis. Adsorbed $\text{NH}_x(\text{s})$ species then dominate the steady-state formation of NH_3 via Eley-Rideal (E-R) reactions. Regarding the role of Ar in increasing the NH_3 synthesis rate, analysis of the modeling results reveals that the Ar contributions originate from excited Ar species in the 4s state. Moreover, charge transfer reactions between Ar^+ and N_2 , when followed by dissociative recombination of N_2^+ , are not a significant source of gas-phase N radical production under the given conditions, which is dominated by electron-impact dissociation of N_2 . Thus the model predicts that argon is unlikely to have a dominant effect on the efficiency of NH_3 formation via a chemical pathway due to the dominant role of electrons in this process under most conditions. Instead, experimentally observed enhancement in NH_3 production upon Ar dilution may be due to both changes to the chemistry and the electron number density and reduced electric field in the discharge. The utilization of Ar to optimize plasma discharge conditions and produce electronically excited gas-phase N_2 molecules under the presence of catalysts are future subjects of investigation.

Acknowledgment

This material is based upon work supported by the U.S. Department of Energy, Office of Science, Office of Fusion Energy Sciences under award number DE-SC0020233.

References

- (1) Hong, J.; Pancheshnyi, S.; Tam, E.; Lowke, J. J.; Praver, S.; Murphy, A. B. Kinetic Modelling of NH_3 Production in $\text{N}_2\text{-H}_2$ Non-Equilibrium Atmospheric-Pressure Plasma Catalysis. *J. Phys. D: Appl. Phys.* **2017**, *50* (15), 154005. <https://doi.org/10.1088/1361-6463/aa6229>.
- (2) Wang, Y.; Craven, M.; Yu, X.; Ding, J.; Bryant, P.; Huang, J.; Tu, X. Plasma-Enhanced Catalytic Synthesis of Ammonia over a $\text{Ni}/\text{Al}_2\text{O}_3$ Catalyst at Near-Room Temperature: Insights into the Importance of the Catalyst Surface on the Reaction Mechanism. *ACS Catal.* **2019**, *9* (12), 10780–10793. <https://doi.org/10.1021/acscatal.9b02538>.

- (3) Bruggeman, P.; Brandenburg, R. Atmospheric Pressure Discharge Filaments and Microplasmas: Physics, Chemistry and Diagnostics. *J. Phys. D: Appl. Phys.* **2013**, *46* (46), 464001. <https://doi.org/10.1088/0022-3727/46/46/464001>.
- (4) Xu, X. Dielectric Barrier Discharge — Properties and Applications. *Thin Solid Films* **2001**, *390* (1), 237–242. [https://doi.org/10.1016/S0040-6090\(01\)00956-7](https://doi.org/10.1016/S0040-6090(01)00956-7).
- (5) Vojvodic, A.; Medford, A. J.; Studt, F.; Abild-Pedersen, F.; Khan, T. S.; Bligaard, T.; Nørskov, J. K. Exploring the Limits: A Low-Pressure, Low-Temperature Haber–Bosch Process. *Chemical Physics Letters* **2014**, *598*, 108–112. <https://doi.org/10.1016/j.cplett.2014.03.003>.
- (6) Mehta, P.; Barboun, P.; Herrera, F. A.; Kim, J.; Rumbach, P.; Go, D. B.; Hicks, J. C.; Schneider, W. F. Overcoming Ammonia Synthesis Scaling Relations with Plasma-Enabled Catalysis. *Nature Catalysis* **2018**, *1* (4), 269–275. <https://doi.org/10.1038/s41929-018-0045-1>.
- (7) Liu, T.-W.; Gorky, F.; Carreon, M. L.; Gómez-Gualdrón, D. A. Energetics of Reaction Pathways Enabled by N and H Radicals during Catalytic, Plasma-Assisted NH₃ Synthesis. *ACS Sustainable Chem. Eng.* **2022**, *10* (6), 2034–2051. <https://doi.org/10.1021/acssuschemeng.1c05660>.
- (8) Iwamoto, M.; Akiyama, M.; Aihara, K.; Deguchi, T. Ammonia Synthesis on Wool-Like Au, Pt, Pd, Ag, or Cu Electrode Catalysts in Nonthermal Atmospheric-Pressure Plasma of N₂ and H₂. *ACS Catal.* **2017**, *7* (10), 6924–6929. <https://doi.org/10.1021/acscatal.7b01624>.
- (9) Peng, P.; Li, Y.; Cheng, Y.; Deng, S.; Chen, P.; Ruan, R. Atmospheric Pressure Ammonia Synthesis Using Non-Thermal Plasma Assisted Catalysis. *Plasma Chem Plasma Process* **2016**, *36* (5), 1201–1210. <https://doi.org/10.1007/s11090-016-9713-6>.
- (10) Hong, J.; Aramesh, M.; Shimoni, O.; Seo, D. H.; Yick, S.; Greig, A.; Charles, C.; Prawer, S.; Murphy, A. B. Plasma Catalytic Synthesis of Ammonia Using Functionalized-Carbon Coatings in an Atmospheric-Pressure Non-Equilibrium Discharge. *Plasma Chem Plasma Process* **2016**, *36* (4), 917–940. <https://doi.org/10.1007/s11090-016-9711-8>.
- (11) Liu, Y.; Wang, C.-W.; Xu, X.-F.; Liu, B.-W.; Zhang, G.-M.; Liu, Z.-W.; Chen, Q.; Zhang, H.-B. Synergistic Effect of Co–Ni Bimetal on Plasma Catalytic Ammonia Synthesis. *Plasma Chem Plasma Process* **2022**, *42* (2), 267–282. <https://doi.org/10.1007/s11090-021-10223-1>.
- (12) Akay, G.; Zhang, K. Process Intensification in Ammonia Synthesis Using Novel Coassembled Supported Microporous Catalysts Promoted by Nonthermal Plasma. *Ind. Eng. Chem. Res.* **2017**, *56* (2), 457–468. <https://doi.org/10.1021/acs.iecr.6b02053>.
- (13) Yin, K. S.; Venugopalan, M. Plasma Chemical Synthesis. I. Effect of Electrode Material on the Synthesis of Ammonia. *Plasma Chem Plasma Process* **1983**, *3* (3), 343–350. <https://doi.org/10.1007/BF00564632>.
- (14) Mizushima, T.; Matsumoto, K.; Sugoh, J.; Ohkita, H.; Kakuta, N. Tubular Membrane-like Catalyst for Reactor with Dielectric-Barrier-Discharge Plasma and Its Performance in Ammonia Synthesis. *Applied Catalysis A: General* **2004**, *265* (1), 53–59. <https://doi.org/10.1016/j.apcata.2004.01.002>.
- (15) Chen, Z.; Koel, B. E.; Sundaresan, S. Plasma-Assisted Catalysis for Ammonia Synthesis in a Dielectric Barrier Discharge Reactor: Key Surface Reaction Steps and Potential Causes of Low Energy Yield. *J. Phys. D: Appl. Phys.* **2021**, *55* (5), 055202. <https://doi.org/10.1088/1361-6463/ac2f12>.

- (16) Chen, Z.; Jaiswal, S.; Diallo, A.; Sundaresan, S.; Koel, B. E. Effect of Porous Catalyst Support on Plasma-Assisted Catalysis for Ammonia Synthesis. *J. Phys. Chem. A* **2022**, *126* (46), 8741–8752. <https://doi.org/10.1021/acs.jpca.2c05023>.
- (17) Seol, Y.; Chang, H. Y.; Ahn, S. K.; You, S. J. Study on Characteristics of Electron Parameters on Inert Gas Addition in a Capacitively Coupled SF₆/O₂ Plasma. *AIP Advances* **2022**, *12* (12), 125117. <https://doi.org/10.1063/5.0127857>.
- (18) Taylor, K. J.; Tynan, G. R. Control of Dissociation by Varying Oxygen Pressure in Noble Gas Admixtures for Plasma Processing. *Journal of Vacuum Science & Technology A* **2005**, *23* (4), 643–650. <https://doi.org/10.1116/1.1931682>.
- (19) Taylor, K. J.; Yun, S.; Tynan, G. R. Control of Plasma Parameters by Using Noble Gas Admixtures. *Journal of Vacuum Science & Technology A* **2004**, *22* (5), 2131–2138. <https://doi.org/10.1116/1.1772375>.
- (20) Qayyum, A.; Zeb, S.; Naveed, M. A.; Rehman, N. U.; Ghauri, S. A.; Zakaullah, M. Optical Emission Spectroscopy of Ar–N₂ Mixture Plasma. *Journal of Quantitative Spectroscopy and Radiative Transfer* **2007**, *107* (3), 361–371. <https://doi.org/10.1016/j.jqsrt.2007.02.008>.
- (21) Rehman, N. U.; Anjum, Z.; Masood, A.; Farooq, M.; Ahmad, I.; Zakaullah, M. Metrology of Non-Thermal Capacitively Coupled N₂–Ar Mixture Plasma. *Optics Communications* **2013**, *296*, 72–78. <https://doi.org/10.1016/j.optcom.2013.01.004>.
- (22) Karnopp, J.; Magaldi, B.; Sagás, J.; Pessoa, R. The Effect of Excited Species on the Collisional Energy of Argon Inductively Coupled Plasmas: A Global Model Study. *Plasma* **2022**, *5* (1), 30–43. <https://doi.org/10.3390/plasma5010003>.
- (23) Gorky, F.; Lucero, J. M.; Crawford, J. M.; Blake, B.; Carreon, M. A.; Carreon, M. L. Plasma-Induced Catalytic Conversion of Nitrogen and Hydrogen to Ammonia over Zeolitic Imidazolate Frameworks ZIF-8 and ZIF-67. *ACS Appl. Mater. Interfaces* **2021**, *13* (18), 21338–21348. <https://doi.org/10.1021/acsami.1c03115>.
- (24) Nakajima, J.; Sekiguchi, H. Synthesis of Ammonia Using Microwave Discharge at Atmospheric Pressure. *Thin Solid Films* **2008**, *516* (13), 4446–4451. <https://doi.org/10.1016/j.tsf.2007.10.053>.
- (25) Liu, J.; Zhu, X.; Hu, X.; Zhang, F.; Tu, X. Plasma-Assisted Ammonia Synthesis in a Packed-Bed Dielectric Barrier Discharge Reactor: Effect of Argon Addition. *Vacuum* **2022**, *197*, 110786. <https://doi.org/10.1016/j.vacuum.2021.110786>.
- (26) Ben Yaala, M.; Scherrer, D.-F.; Saeedi, A.; Moser, L.; Soni, K.; Steiner, R.; De Temmerman, G.; Oberkofler, M.; Marot, L.; Meyer, E. Plasma-Activated Catalytic Formation of Ammonia from N₂–H₂: Influence of Temperature and Noble Gas Addition. *Nuclear Fusion* **2020**, *60* (1), 016026. <https://doi.org/10.1088/1741-4326/ab519c>.
- (27) Bogaerts, A. Hybrid Monte Carlo — Fluid Model for Studying the Effects of Nitrogen Addition to Argon Glow Discharges. *Spectrochimica Acta Part B: Atomic Spectroscopy* **2009**, *64* (2), 126–140. <https://doi.org/10.1016/j.sab.2008.11.004>.
- (28) Kang, N.; Gaboriau, F.; Oh, S.; Ricard, A. Modeling and Experimental Study of Molecular Nitrogen Dissociation in an Ar–N₂ ICP Discharge. *Plasma Sources Sci. Technol.* **2011**, *20* (4), 045015. <https://doi.org/10.1088/0963-0252/20/4/045015>.
- (29) Kimura, T.; Kasugai, H. Properties of Inductively Coupled Rf Ar/H₂ Plasmas: Experiment and Global Model. *Journal of Applied Physics* **2010**, *107* (8), 083308. <https://doi.org/10.1063/1.3345084>.

- (30) Kimura, T.; Kasugai, H. Experiments and Global Model of Inductively Coupled Rf Ar/N₂ Discharges. *Journal of Applied Physics* **2010**, *108* (3), 033305. <https://doi.org/10.1063/1.3468603>.
- (31) Sode, M.; Jacob, W.; Schwarz-Selinger, T.; Kersten, H. Measurement and Modeling of Neutral, Radical, and Ion Densities in H₂-N₂-Ar Plasmas. *Journal of Applied Physics* **2015**, *117* (8), 083303. <https://doi.org/10.1063/1.4913623>.
- (32) S. Pancheshnyi, B. Eismann, G.J.M. Hagelaar, L.C. Pitchford, Computer Code ZDPlasKin, <Http://Www.Zdplaskin.Laplace.Univ-Tlse.Fr> (University of Toulouse, LAPLACE, CNRS-UPS-INP, Toulouse, France, 2008).
- (33) Hagelaar, G. J. M.; Pitchford, L. C. Solving the Boltzmann Equation to Obtain Electron Transport Coefficients and Rate Coefficients for Fluid Models. *Plasma Sources Sci. Technol.* **2005**, *14* (4), 722. <https://doi.org/10.1088/0963-0252/14/4/011>.
- (34) BOLSIG+ | *Electron Boltzmann equation solver*. <http://www.bolsig.laplace.univ-tlse.fr/> (accessed 2023-01-26).
- (35) Liang, Y.-S.; Xue, C.; Zhang, Y.-R.; Wang, Y.-N. Investigation of Active Species in Low-Pressure Capacitively Coupled N₂/Ar Plasmas. *Physics of Plasmas* **2021**, *28* (1), 013510. <https://doi.org/10.1063/5.0031120>.
- (36) Arakoni, R. A.; Bhoj, A. N.; Kushner, M. J. H₂ generation in Ar/NH₃ microdischarges. *J. Phys. D: Appl. Phys.* **2007**, *40* (8), 2476–2490. <https://doi.org/10.1088/0022-3727/40/8/010>.
- (37) Mitchell, J. B. A.; Novotny, O.; LeGarrec, J. L.; Florescu-Mitchell, A.; Rebrion-Rowe, C.; Stolyarov, A. V.; Child, M. S.; Svendsen, A.; Ghazaly, M. A. E.; Andersen, L. H. Dissociative Recombination of Rare Gas Hydride Ions: II. ArH⁺. *J. Phys. B: At. Mol. Opt. Phys.* **2005**, *38* (10), L175. <https://doi.org/10.1088/0953-4075/38/10/L07>.
- (38) Anicich, V. G. *An Index of the Literature for Bimolecular Gas Phase Cation-Molecule Reaction Kinetics*; 2003. <https://trs.jpl.nasa.gov/handle/2014/7981> (accessed 2021-05-02).
- (39) Loffhagen, D.; Becker, M. M.; Czerny, A. K.; Klages, C.-P. Modeling of Atmospheric-Pressure Dielectric Barrier Discharges in Argon with Small Admixtures of Tetramethylsilane. *Plasma Chem Plasma Process* **2021**, *41* (1), 289–334. <https://doi.org/10.1007/s11090-020-10121-y>.
- (40) Rimstidt, J. D.; Zhang, Y.; Zhu, C. Rate Equations for Sodium Catalyzed Amorphous Silica Dissolution. *Geochimica et Cosmochimica Acta* **2016**, *195*, 120–125. <https://doi.org/10.1016/j.gca.2016.09.020>.
- (41) Saracino, M.; Pretali, L.; Capobianco, M. L.; Emmi, S. S.; Navacchia, M. L.; Bezzi, F.; Mingazzini, C.; Burrelli, E.; Zanelli, A. Titania Nano-Coated Quartz Wool for the Photocatalytic Mineralisation of Emerging Organic Contaminants. *Water Science and Technology* **2017**, *77* (2), 409–416. <https://doi.org/10.2166/wst.2017.457>.
- (42) Pavlin, M.; Horvat, B.; Frankovič, A.; Ducman, V. Mechanical, Microstructural and Mineralogical Evaluation of Alkali-Activated Waste Glass and Stone Wool. *Ceramics International* **2021**, *47* (11), 15102–15113. <https://doi.org/10.1016/j.ceramint.2021.02.068>.
- (43) Li, Y.; Cheng, J.; Lu, P.; Guo, W.; Wang, Q.; He, C. Quartz-Wool-Supported Surface Dummy Molecularly Imprinted Silica as a Novel Solid-Phase Extraction Sorbent for Determination of Bisphenol A in Water Samples and Orange Juice. *Food Anal. Methods* **2017**, *10* (6), 1922–1930. <https://doi.org/10.1007/s12161-016-0765-2>.
- (44) Rouwenhorst, K. H. R.; Kim, H.-H.; Lefferts, L. Vibrationally Excited Activation of N₂ in Plasma-Enhanced Catalytic Ammonia Synthesis: A Kinetic Analysis. *ACS Sustainable Chem. Eng.* **2019**, *7* (20), 17515–17522. <https://doi.org/10.1021/acssuschemeng.9b04997>.

- (45) Engelman, Y.; van 't Veer, K.; Gorbanev, Y.; Neyts, E. C.; Schneider, W. F.; Bogaerts, A. Plasma Catalysis for Ammonia Synthesis: A Microkinetic Modeling Study on the Contributions of Eley–Rideal Reactions. *ACS Sustainable Chem. Eng.* **2021**, *9* (39), 13151–13163. <https://doi.org/10.1021/acssuschemeng.1c02713>.
- (46) Veer, K. van 't; Reniers, F.; Bogaerts, A. Zero-Dimensional Modeling of Unpacked and Packed Bed Dielectric Barrier Discharges: The Role of Vibrational Kinetics in Ammonia Synthesis. *Plasma Sources Sci. Technol.* **2020**, *29* (4), 045020. <https://doi.org/10.1088/1361-6595/ab7a8a>.